The histone chaperone NASP maintains H3-H4 reservoirs in the early Drosophila embryo

Reyhaneh Tirgar[1], Jonathan P. Davies[1], Lars Plate[1,2], and Jared T. Nordman[1]

[1]Department of Biological Sciences, Vanderbilt University, Nashville, TN, 37212, USA

[2]Department of Chemistry, Vanderbilt University, Nashville, TN, 37212, USA

*Corresponding author: jared.nordman@vanderbilt.edu

ABSTRACT

Histones are essential for chromatin packaging and histone supply must be tightly regulated as excess histones are toxic. To drive the rapid cell cycles of the early embryo, however, excess histones are maternally deposited. Therefore, soluble histones must be buffered by histone chaperones but the chaperone necessary to stabilize soluble H3-H4 pools in the Drosophila embryo has yet to be identified. Here, we show that CG8223, the Drosophila ortholog of NASP, is a H3-H4-specific chaperone in the early embryo. NASP specifically binds to H3-H4 in the early embryo. We demonstrate that, while a *NASP* null mutant is viable in Drosophila, *NASP* is maternal effect lethal gene. Embryos laid by NASP mutant mothers have a reduce rate of hatching and show defects in early embryogenesis. Critically, soluble H3-H4 pools are degraded in embryos laid by NASP mutant mothers. Our work identifies NASP as the critical H3-H4 histone chaperone in the Drosophila embryo.

INTRODUCTION

Histones are small, highly conserved, and positively charged proteins essential for packaging the eukaryotic genome. The core of chromatin is 147bp of DNA wrapped around an octamer of histones H2A, H2B, H3, and H4 (Kornberg 1974; Noll and Kornberg 1977; Arents and Moudrianakis 1993; Luger et al. 1997). Histone occupancy affects nearly every aspect of chromatin metabolism including transcription, DNA replication, DNA repair and DNA packaging (Khorasanizadeh 2004; Bannister and Kouzarides 2011; Talbert and Henikoff 2017; Kornberg and Lorch 2020). Thus, it is crucial that histone expression levels are delicately balanced as histone reduction or overexpression is detrimental to the cell (Meeks-Wagner and Hartwell 1986; Gunjan and Verreault 2003; Singh et al. 2010; Celona et al. 2011; Herrero and Moreno 2011). Exemplifying the importance of histone balance, the production of histones is tightly coordinated with cell cycle progression; histone expression peaks at S phase when the demand for histones is highest (Oliver et al. 1974; Bonner et al. 1988; Osley 1991; Zhao et al. 2000). Furthermore, the soluble pools of histones are less than 1% of the total histone levels in cells and mechanisms exist to degrade and prevent the overabundance of soluble histones (Oliver et al. 1974; Bonner et al. 1988; Gunjan et al. 2006; Marzluff et al. 2008).

Early embryogenesis of many organisms, including Drosophila, presents a challenge to the histone supply and demand paradigm. The early embryo develops extremely rapidly in the first few hours of development (Yuan et al. 2016; Vastenhouw et al. 2019). Prior to the mid blastula transition (MBT), rapid cleavage cycles in the early embryo occur in the absence of gap phases and zygotic transcription (Yuan et al. 2016). Therefore, early embryogenesis must be driven from maternally supplied stockpiles of RNA and protein, including histones (Ambrosio and Schedl

1985; Foe et al. 1993; Walker and Bownes 1998; Horard and Loppin 2015; Song et al. 2017). As opposed to the less than 1% of soluble histones found in somatic cells, early Drosophila embryos have >50% of free histones, which is likely an underestimation when considering the earliest cell cycles (Shindo and Amodeo 2019). Thus, there must be mechanisms present in the early embryo to suppress the toxicity associated with excess histones in somatic cells.

From their molecular birth to their eventual deposition into chromatin, histones are continuously bound by a network of proteins known as histone chaperones (Pardal et al. 2019). Histone chaperones are key for histone stability and affect all aspects of histone metabolism including histone folding, storage, transport, post translational modifications, and histone turnover (Hammond et al. 2017). Importantly, histone chaperones directly or indirectly affect chromatin structure and function by delivery and handoff of histones to other histone chaperones or chromatin-associated factors within a given network, that deposit histones into chromatin (Gurard-Levin et al. 2014). While a few chaperones can bind all histones, most histone chaperones bind specifically to H3-H4 or H2A-H2B (Natsume et al. 2007; Ramos et al. 2010; Elsässer et al. 2012; Hammond et al. 2017). In Drosophila embryos, the histone chaperone Jabba sequesters histones H2A-H2B to lipid droplets and protects H2A and H2B from degradation (Li et al. 2012). It is still unknown however what histone chaperone protects soluble H3 and H4 pools in the early embryo. While there are multiple H3-H4-specific histone chaperones, nuclear autoantigenic sperm protein (NASP) is an alluring candidate to chaperone H3-H4 in Drosophila embryos as NASP is known to maintain a soluble reservoir of histone H3-H4 in mammalian cells (Cook et al. 2011; Horard and Loppin 2015). Furthermore, the Xenopus NASP homolog N1/N2 associates with soluble pools of H3 and H4 in egg lysates (Kleinschmidt et al. 1985). Lastly, *NASP*

is essential for embryonic development in mammals (Richardson et al. 2006; Nagatomo et al. 2016). Thus, we hypothesized that NASP is a histone H3-H4 chaperone in the early embryo.

Here, based on sequence and structure, we identified CG8223 as the Drosophila NASP homolog. We show that CG8223/NASP specifically binds to histones H3-H4 in vivo. We demonstrate that NASP is a maternal effect lethal gene in Drosophila and that embryos laid by *NASP* mutant mothers have impaired development. Finally, we show that in the absence of NASP, soluble H3 and H4 levels decrease in both eggs and embryos. Overall, our findings demonstrate that NASP protects soluble pools of H3-H4 from degradation in Drosophila embryos.

RESULTS

Drosophila melanogaster CG8223 is the histone H3-H4 chaperone NASP

Histone supply is carefully controlled to prevent the toxicity associated with excess histones (Meeks-Wagner and Hartwell 1986; Gunjan and Verreault 2003; Gunjan et al. 2006; Singh et al. 2009; Herrero and Moreno 2011). In rapidly developing embryos, however, excess histones are maternally deposited to fuel the rapid cell cycles of the early embryo (Ambrosio and Schedl 1985; Walker and Bownes 1998; Horard and Loppin 2015). To prevent histone toxicity, excess histones must be chaperoned by H2A-H2B or H3-H4-specific chaperones (Berloco et al. 2001; Günesdogan et al. 2010). In Drosophila, Jabba serves as the major H2A-H2B-specific chaperone, but the H3-H4-specific chaperone has yet to be identified(Li et al. 2012). NASP, Nuclear Autoantigenic Sperm Protein, is an H3-H4-specific chaperone known to buffer excess H3-H4 supply in mammalian cells and Xenopus (Kleinschmidt et al. 1985; Cook et al. 2011). Previous work has identified CG8223 as a possible NASP homolog based on the conserved

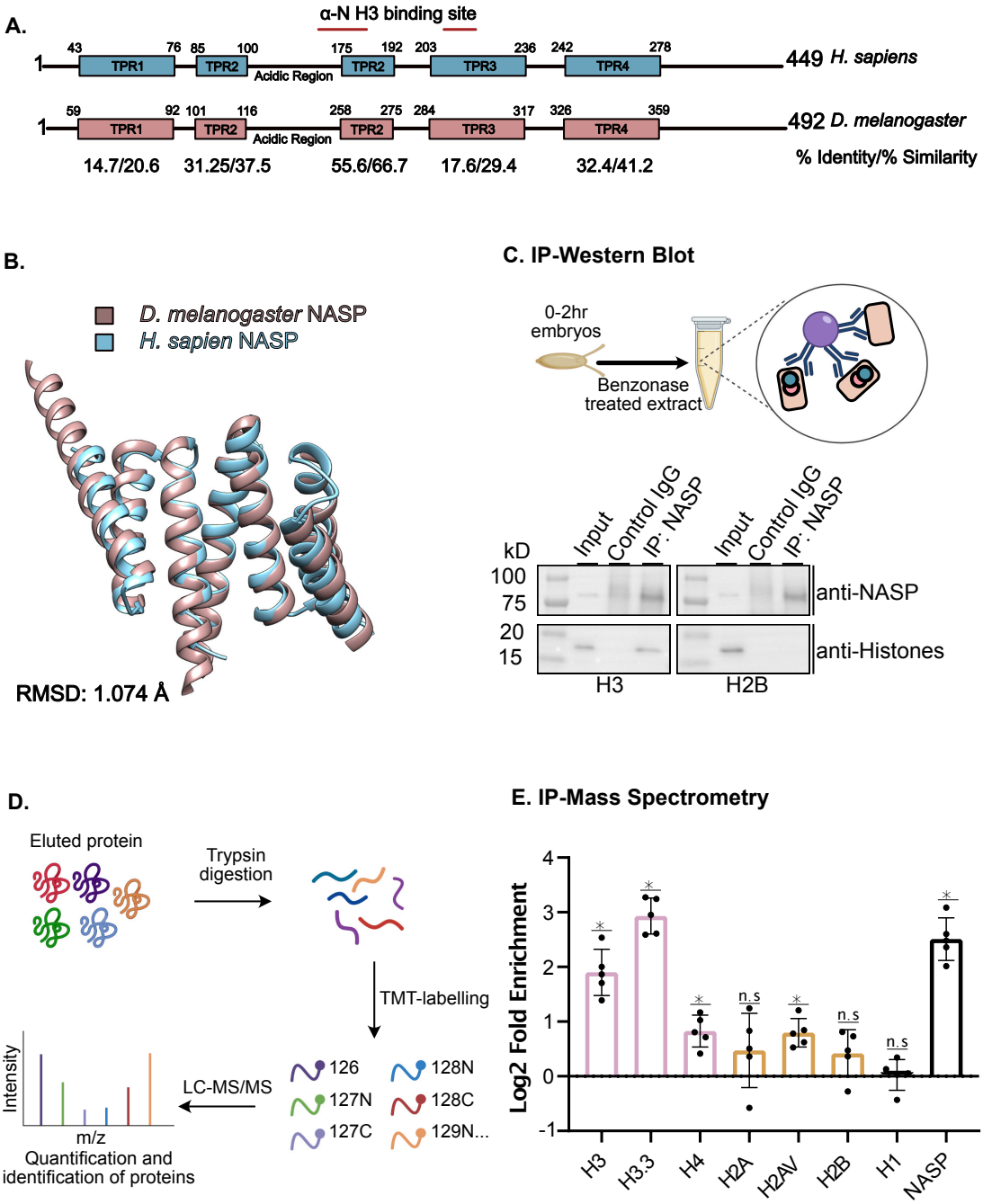

Figure 1. *Drosophila melanogaster* CG8223 is the Histone H3/H4 chaperone NASP. (a) Schematic of *Homo sapiens* and *Drosophila melanogaster* NASP proteins with TPR domains. Below are the calculated % identity/%similarity for each TPR domains. Red lines indicate the location of residues responsible for binding H3. For specific residues see Supplemental Fig 1b. **(b)** Superimposition of *Homo sapiens* NASP (as determined by crystallography) with *Drosophila melanogaster* NASP (predicted by AlphaFold). **(c)** Immunoprecipitation of NASP from 0-2hr AEL embryos. **(d)** Schematic of IP quantitative mass spectrometry approach to quantify NASP-associated proteins. **(e)** Average Log2 fold change for five biological replicates of NASP IP-mass spectrometry relative to IgG control in 0-2hr AEL embryos. Multiple t-test was performed to determine significance ($p<0.05$).

Tetratricopeptide (TRP) motifs, which are found in NASP homologs (Nabeel-Shah et al. 2014). To verify that CG8223 is in fact NASP, we searched the Drosophila proteome for a homolog of human NASP and identified CG8223 as the one and only putative NASP homolog. Alignment of CG8223 with human NASP revealed a similar domain structure with 28% identity (S1A Fig). Critically, the regions of CG8223 with the highest degree of conservation to human NASP are the regions known to bind to H3 directly (Fig 1A). Furthermore, a structural prediction of CG8223 (excluding the dimerization domain, α-89) is highly similar to a recent human crystal structure of sNASP, with an 1.074 angstrom RMSD value (Fig 1B)(Bao et al. 2022).

To test experimentally whether CG8223 is an H3-H4-specific binding protein in vivo, we immunoprecipitated (IP) CG8223 from embryo extracts (0-2h AEL) using a CG8223-specific antibody(S1E Fig). Western blot analysis of the IP revealed that CG8223 and Histone H3, but not H2B, are in the same protein complex (Fig 1C). To extend this analysis beyond H3 and H2B, we used IP coupled to quantitative mass spectrometry to determine which canonical histones and histone variants complex with CG8223. To this end, precipitated material was labelled with tandem mass tag (TMT) and only peptides that were unique to each histone were quantified (Fig 1D). This analysis revealed that CG8223 associates with H3, H4 and H3.3. CG8223 does not, however, associate with H2A or H2B (Fig 1E). Interestingly, we identified an association between NASP and the H2A variant, H2Av Based on the conservation, structural similarity and in vivo association with H3-H4, we conclude that CG8223 is the sole Drosophila NASP homolog, which we will now refer to as NASP.

NASP is a maternal effect lethal gene

Now that we have established NASP as an H3-H-specific binding protein in Drosophila, we wanted to ask how *NASP* affects Drosophila development. We used CRISPR-based mutagenesis to target exon 2 to generate *NASP* mutants. From this approach, we recovered two mutants; *NASP*^{1} and *NASP*^{2} (Fig 2A). The *NASP*^{1} allele contains a 6bp insertion resulting in a two amino acid insertion at amino acid 203. Given this small insertion is in a non-conserved region of the protein, it is not predicted to affect NASP function (S1B Fig). In contrast, the *NASP*^{2} allele contains a 4bp deletion

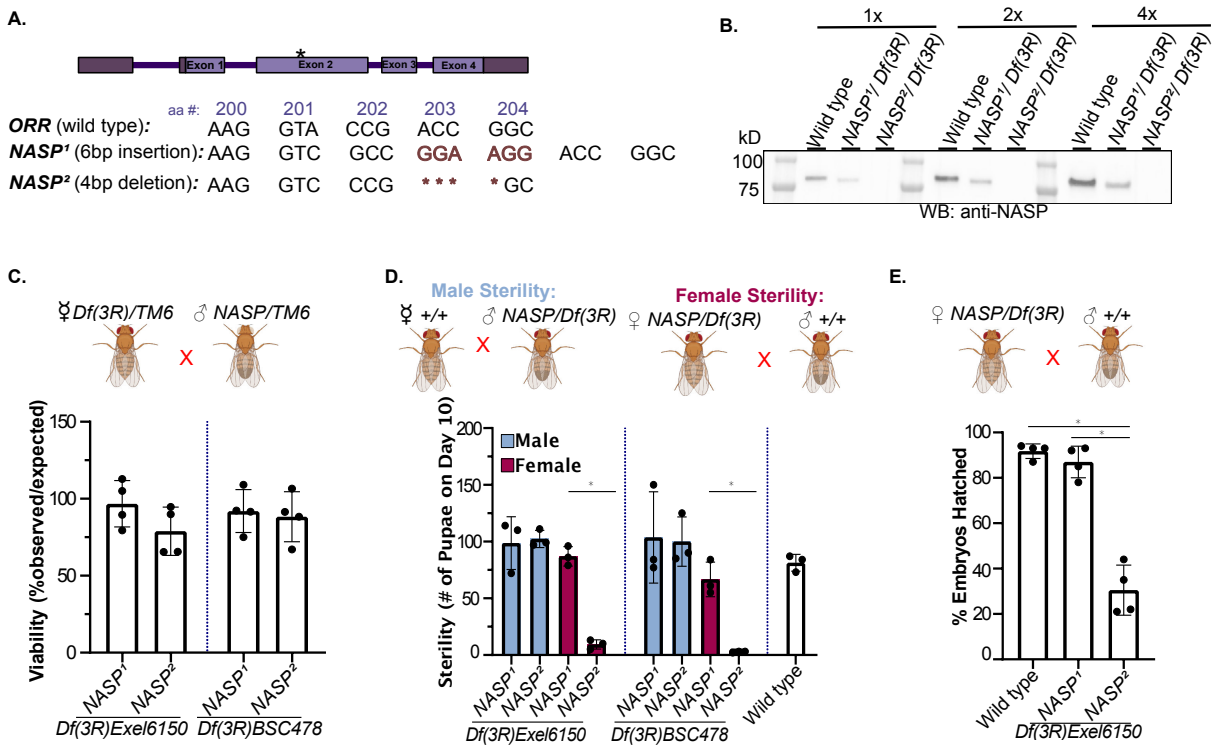

Figure 2. *NASP* is a maternal effect lethal gene. (a) Schematic of *NASP*^{1} and NASP ^{2} CRISPR mutants. **(b)** Western blot analysis of ovary extracts from the indicated genotypes with total protein loading control. *NASP*^{1}*/Df(3R)Exel6150* has less NASP due to a reduction in gene dose. **(c)** The percentage of progeny observed with the appropriate genotype (as shown on the x-axis) over the expected percentage. Each data point is representative of a biological replicate (n=4). Unpaired t-test was used to determine significance ($p<0.05$). **(d)** The number of pupae on day 10 produced from females with the genotypes outlined on the x-axis crossed with wild type males. Each data point is representative of a biological replicate (n=3). Unpaired t-test was used to determine significance ($p<0.05$). **(e)** Percentage of embryos hatched laid by wild type, *NASP*^{1}*/Df(3R)Exel6150* or *NASP*^{2}*/Df(3R)Exel6150* mothers. Each data point is representative of a biological replicate (n=4) and represents the hatch rate of a group of 100 embryos. Dunn's Multiple Comparison post-hoc was performed to determine significance ($p<0.05$).

158 that results in a frameshift starting at amino acid 203 and a truncation of NASP (Fig 2A). Western
159 blot analysis of ovary extracts derived from wild type, *NASP*^{1} or *NASP*^{2} mutants revealed that
160 there was no detectable NASP^{2} protein even with 4X the protein loaded. In contrast, however,
161 the NASP^{1} protein was stable (Fig 2B).

162 To examine viability of the *NASP* mutants, we counted the number of *NASP* mutant
163 progeny relative to the expected frequency (Fig 2C). To account for any CRISPR off target effects,
164 we performed all crosses with two independent deficiency lines (see methods) to generate
165 compound heterozygous mutants. Crossing *NASP*^{1} or *NASP*^{2} mutants with either deficiency line
166 revealed that both *NASP*^{1} *and NASP*^{2} mutants are viable (Fig 2C).

167 Although the *NASP*^{2} mutant is viable, it had a lower fecundity, and we were unable to
168 maintain a stock. Thus, we hypothesized that the *NASP*^{2} mutant is either male or female sterile.
169 To test this hypothesis, we measured the number of pupae formed 10 days after egg laying (AEL)
170 from *NASP* mutant parents. *NASP*^{2} mutant mothers produced a significantly lower number of
171 pupae compared to both wild type and the *NASP*^{1} mutant mothers (Fig 2D). There was no
172 significant difference in the number of progeny produced when wild type females were crossed
173 to male *NASP*^{2} mutants, indicating that loss of NASP function results in female sterility (Fig 2D).
174 Results were consistent for both compound heterozygous from two independent deficiency lines
175 (Fig 2D).

176 Previous proteomic studies revealed NASP to be at replication forks in Drosophila cultured
177 S2 cells, Drosophila embryos, and human cells (Wessel et al. 2019; Munden et al. 2022).
178 Therefore, it is possible that NASP may function during chorion gene amplification in follicle cells,
179 which is critical to produce egg shell protein in a short developmental window (Spradling and

Mahowald 1980). To test this, we measured DNA copy number at the highest amplified region ,DAFC-66D, in stage 12 egg chambers. The *NASP*^{2} mutant did not show a significant difference in amplification (S2A Fig). Therefore, we conclude that the female sterility associated with the *NASP*^{2} mutant is independent of gene amplification.

Although *NASP*^{2} mutants were viable, embryos laid by *NASP*^{2} mutant mothers showed a significantly lower hatching percentage compared to *NASP*^{1} and wild type (Fig 2E). To ask whether maternally supplied NASP is essential for embryogenesis, we ensured that all progeny have at least one copy of *NASP* by crossing *NASP*^{2} virgin females with wild type males. Interestingly, even when the progeny had a functional *NASP* allele, there was a significantly lower number of progeny compared to crosses with wild type females (S2B Fig). Furthermore, embryos laid by NASP mutant mothers crossed with wild type males had a significant reduction in hatching rate (S2C Fig). Therefore, we conclude that *NASP* is a maternal effect lethal gene.

NASP stabilizes H3-H4 reservoirs in the early Drosophila embryo

Since *NASP* is a maternal effect lethal gene, and embryos laid by *NASP* mutant mothers fail to hatch, embryos laid by NASP mutant mothers are likely devoid of a key factor(s) necessary for development. Given that NASP is a H3-H4-specific chaperone, we hypothesized that H3-H4 reservoirs are destabilized in embryos laid by NASP mutant mothers. We used Western blotting to measure H3 and H2B levels in embryos collected from *NASP*^{2} or wild type mothers. Qualitatively, embryos laid by *NASP*^{2} mothers had lower levels of H3, but not H2B, when compared to embryos laid by wild type mothers (Fig 3A). To determine when in development H3 pools begin to be degraded in the absence of NASP, we performed Western blot analysis of H3

and H2B in stage 14 egg chambers dissected from *NASP²* and wild type mothers. H3, but not H2B, levels were slightly decreased in stage 14 egg chambers (Fig 3B). Thus, we conclude that NASP is critical for H3 stabilization during oogenesis and embryogenesis.

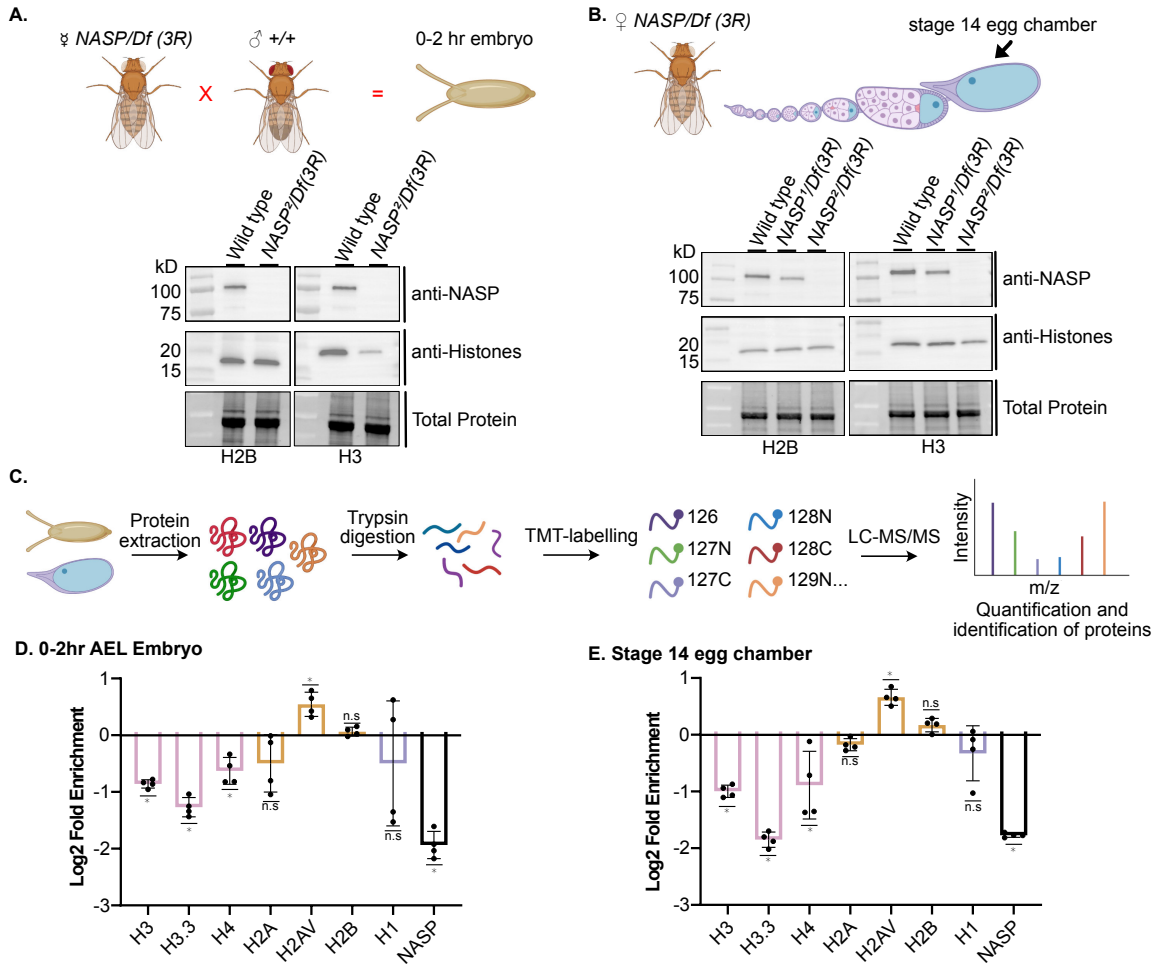

Figure 3. NASP stabilizes H3/H4 reservoirs in the early Drosophila embryo. (a) Western blot analysis of 0-2hr AEL embryos laid by wild type or *NASP²/Df(3R)Exel6150* mutant mothers. **(b)** Western blot analysis wild type or *NASP²/Df(3R)Exel6150* stage 14 egg chamber. **(c)** Schematic of quantitative mass spectrometry approach to quantify protein abundance. **(d)** Average Log2 fold change for four biological replicates of unique peptides corresponding to H2A, H2AV, H2B, H3, H3.3, H4, H1, and NASP in 0-2hr AEL embryos laid by *NASP²/Df(3R)Exel6150* or wild type mothers. Adjusted p-values were calculated by performing multiple t-tests with a Holm-Sidak correction ($p<0.05$). **(e)** Average Log2 fold change for four biological replicates of unique peptides for H2A, H2AV, H2B, H3, H3.3, H4, H1, and NASP in *NASP²/Df(3R)Exel6150* or wild type stage 14 egg chambers. Adjusted p-values were calculated by performing multiple t-tests with a Holm-Sidak correction ($p<0.05$).

To extend this analysis to all canonical and variant histones and gain a quantitative view of histone levels during development, we used quantitative mass spectrometry to measure

histone levels in early embryos and stage 14 egg chambers (Fig 3C). To this end, we TMT labeled extracts from 0-2 hour (AEL) embryos and stage 14 egg chambers from four biological replicates. This analysis revealed that the levels of histones H3, H3.3, and H4 were significantly reduced in embryos laid by *NASP*^{2} mutant mothers and in *NASP*^{2} mutant stage 14 egg chambers (Fig 3D, E). H1, H2A and H2B levels were stable while H2Av levels increased (Fig 3D,E). Overall, quantitative mass spectrometry reveals that in the absence of NASP, H3 and H4 are destabilized starting in oogenesis. Thus, we conclude that NASP stabilizes H3-H4 reservoirs during both oogenesis and embryogenesis.

Embryos laid by *NASP* mutant mothers stall or slow in early embryogenesis

60-70% of embryos laid by *NASP* mutant mothers do not hatch. To determine what the underlying defects are in embryogenesis, we DAPI stained 0-4 AEL embryos and manually scored the number of embryos in each cell cycle. We observed that 72% of embryos laid by *NASP* mutant mothers were in cell cycles 1-11 whereas only 34% of wild type embryos were in cycles 1-11 (Fig 4A). Further, fewer embryos laid by *NASP* mutant mothers surpassed cell cycle 14. Previously, maternal knockdown of CG8223 led to 61% of embryos to cell cycle arrest in stage 2 (Zhang et al. 2018). This suggests that embryos laid by *NASP* mutant mothers progress more slowly or are stalled in early embryonic cycles.

To determine if the absence of NASP caused further defects in embryogenesis, we quantified the number of embryos that contained morphological defects. We found that 45% of embryos laid by *NASP* mutant mothers had atypical morphology compared to only 5% in wild type embryos. Together, we conclude that embryos laid by NASP mutant mothers have defects

239 starting early in embryogenesis, likely slowing or stalling the early cell cycles and causing gross
240 morphological defects.

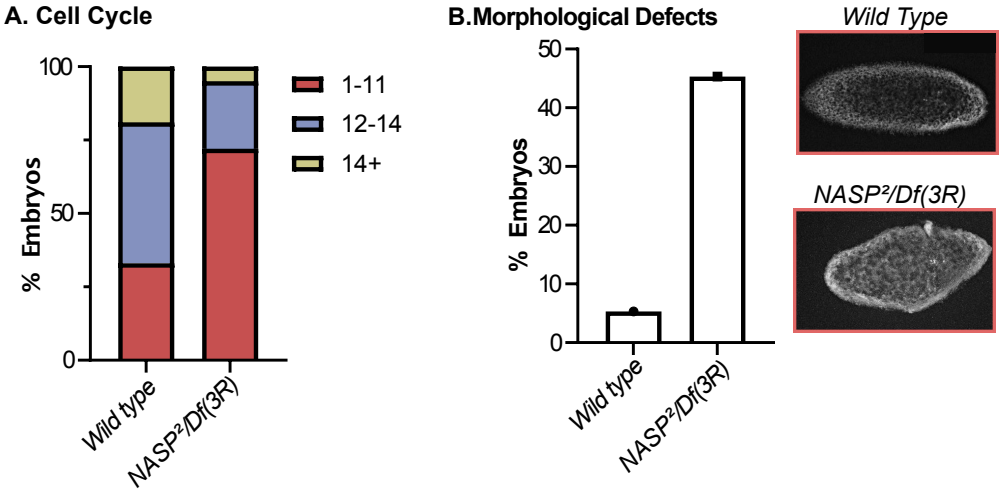

241

242 **Figure 4. Embryos laid by *NASP* mutant mothers stall or slow in early embryogenesis (a)** Percentage of 0-4hr AEL embryos in
243 respective cell cycles (n=75). **(b)** Percentage of 0-4hr AEL embryos with morphological defects (n=75) for embryos laid by wild
244 type or *NASP²/Df(3R)Exel6150* mutant mothers. Representative images of DAPI stained from embryos laid by wild type or
245 *NASP²/Df(3R)Exel6150* mutant mothers.
246

247 **DISCUSSION**

248 Early Drosophila embryogenesis provides a unique challenge to histone supply and
249 demand. The early embryo is maternally stockpiled with an overabundance of histones, yet
250 overproduction of histones is detrimental to cells (Berloco et al. 2001; Gunjan and Verreault
251 2003; Singh et al. 2010; Celona et al. 2011; Herrero and Moreno 2011). Excess histone supply is
252 likely tolerated through the activity of histone chaperones (Li et al. 2012; Horard and Loppin
253 2015). The histone chaperone Jabba stabilizes soluble H2A-H2B pools in the early embryo by
254 sequestering histones to lipid droplets (Li et al. 2012). The histone chaperone that maintains
255 soluble H3-H4 pools in the early Drosophila embryo, however, has yet to be identified. Our work
256 demonstrates that CG8223, the Drosophila homolog of NASP, is a H3-H4 chaperone in the early

257 embryo. This conclusion is supported by several independent lines of evidence. First, NASP
258 associates with H3-H4, but not H2A-H2B in vivo. Second, soluble pools of H3-H4, but not H2A-
259 H2B, are destabilized in the absence of NASP. Third, *NASP* is a maternal effect lethal gene and
260 embryos laid by NASP mutant mothers have defects in embryonic development and embryo
261 hatching. Taken together, we conclude that NASP is the predominant H3-H4 chaperone in the
262 early Drosophila embryo.

263 Embryos laid by *NASP* mutant mothers have defects in embryogenesis. We do not
264 currently know, however, what specific molecular mechanism(s) underlie these defects. There
265 are several non-mutually exclusive mechanisms that could explain the defects we observe in
266 embryogenesis. One possibility is that the H3-H4 supply is insufficient to fuel the demand for
267 chromatin formation in the early embryo. In the early embryo, a single nucleus must rapidly
268 expand to ~8,000 nuclei in two hours (Yuan et al. 2016). To keep up with the demand for
269 chromatin formation, the early embryo is likely dependent on the maternally loaded histones. In
270 the absence of maternally deposited NASP, H3 and H4 pools are substantially reduced. Thus, it is
271 possible that embryos laid by *NASP* mutant mothers simply lack sufficient H3 and H4 supplies for
272 rapid chromatin formation.

273 Reduced soluble pools of H3-H4 have the potential to impact cell cycle dynamics in the
274 early embryo. Overexpression of the N-terminal tail of H3 delays Chk1 activation, thereby
275 influencing cell cycle length and the onset of the MBT (Shindo and Amodeo 2021). Therefore,
276 soluble H3 pools could act as a timer to prevent Chk1 activation and promote rapid cell cycles.
277 Decreasing soluble H3 pools during embryogenesis could allow Chk1 to be prematurely activated

and cell cycle length to be extended, thereby altering key cell cycle events in the early embryo and the onset of the MBT (Chari et al. 2019).

Proper chromatin packaging requires an equimolar ratio of histones (Camerini-Otero et al. 1976). In *C. elegans*, depletion of embryonic H2B levels results in animal sterility. Interestingly, this sterility can be suppressed by reducing H3-H4 levels (Zhao et al. 2022) . Therefore, proper stoichiometry of histones, rather than absolute histone levels, is critical for embryo viability (Meeks-Wagner and Hartwell 1986; Au et al. 2008). Embryos laid by *NASP* mutant mothers have reduced H3 and H4 levels yet H2A and H2B levels remain unaffected. It is possible that this alteration in histone stoichiometry leads to both female sterility and defects in embryo development. Similarly, embryos laid by NASP mutant mothers have increased H2Av levels. While it is unclear how NASP would directly or indirectly destabilize H2Av, overexpression of H2Av causes nuclear fallout and reduced hatching rate (Li et al. 2014). Thus, the increased H2Av levels in embryos laid by NASP mutant mothers could contribute to defects in embryo development. Finally, while imbalances in soluble histone pools likely contribute to defects during embryogenesis, we cannot rule out the possibility that female sterility in the NASP mutant is causes by changes in the level of a non-histone protein.

It is still unresolved what mechanism is responsible for histone degradation in embryos laid by *NASP* mutant mothers and when in development histone degradation begins. Our work shows that H3-H4 levels are already reduced in the latest stage of oogenesis. Therefore, histone degradation likely begins during oogenesis. Previous work in mammalian cells demonstrated that autophagy is responsible for degrading excess H3 and H4 upon NASP depletion (Cook et al. 2011). Therefore, it is possible that, in Drosophila, autophagy is responsible for H3-H4 degradation in

the absence of NASP. In late-stage egg chambers and early embryos, we were still able to detect H3 and H4, indicating that H3-H4 pools are not completely degraded in the absence of NASP. While there could be another chaperone stabilizing H3 and H4, that chaperone would only be capable of stabilizing a small fraction of the total H3-H4 pools. While this chaperone could stabilize a fraction of the total H3-H4 pools, that is not sufficient to drive embryogenesis. Further, this small fraction of soluble histones could be the result of up regulated translation in the early embryo. Now that we have identified NASP as the missing H3-H4-specific chaperone necessary to stabilize soluble H3-H4 pools during Drosophila embryogenesis, we will be able to begin to address fundamental questions about histone storage and stability during oogenesis and embryogenesis.

METHODS

Resources Table

Reagent	Source	Identifier	Additional information
Antibodies			
NASP	This Study	--	1:2000
H3	Abcam	ab21054	1:1000
H2B	Abcam	ab52484	1:1000
Peroxidase AffiniPure Donkey Anti-Mouse IgG (H+L)	Jackson ImmunoResearch	715-035-150	1:20,000
Peroxidase AffiniPure Donkey Anti-Rabbit IgG (H+L)	Jackson ImmunoResearch	711-035-152	1:25,000
Strains			
Oregon R	Terry Orr-Weaver	JTN110	--

NASP[1]/TM6	This Study	JTN403	--
NASP[2]/TM6	This Study	JTN404	--
w[1118]; Df(3R)BSC478/TM6C, Sb[1] cu[1	Bloomington Stock Center	24982	--
w[1118]; Df(3R)Exel6150, P{w[+mC]=XP-U}Exel6150/TM6B, Tb[1]	Bloomington Stock Center	7629	--
Primers			
CG8223 CRISPR Forward	IDT	JNpr667	GAAGATGGAGCGGCTAAGAAG
CG8223 CRISPR Reverse	IDT	JNpr668	TGGAACAACTAGCTGTGACCTC
Polymerase alpha site Forward	IDT	JNpr481	CGCCACCTACAACAGCAGAAAA
Polymerase alpha site Reverse	IDT	JNpr482	GGCTACGGTACAGGGGAGTTGA
DAFC-66D site Forward	IDT	JNpr581	GCAGTGGCCTGAAAATTCTGCT
DAFC-66D site Reverse	IDT	JNpr582	AGCTTAGTGCGGCAGTTTGGAA
Software			
Graphpad Prism	--	https://www.graphpad.com/	--
Jalview	Open source	https://www.jalview.org/	--
PDB-TOOLS	Open source	https://wenmr.science.uu.nl/pdbtools/submit	--
Chimera	Open source	https://www.cgl.ucsf.edu/chimera/	--
Fiji	Open source	https://fiji.sc/	

313

314 **Strain list**

315 Wild type – Oregon R (OrR)

316 NASP null mutant ($NASP^2$)- w[1118]; Df(3R)Exel6150, P{w[+mC]=XP-U}Exel6150/TM6B,

317 Tb[1]/$NASP^2$ or w[1118]; Df(3R)BSC478/TM6C, Sb[1] cu[1]/$NASP^2$

318 NASP control mutant ($NASP^1$)- w[1118]; Df(3R)Exel6150, P{w[+mC]=XP-U}Exel6150/TM6B,

319 Tb[1]/$NASP^1$ or w[1118]; Df(3R)BSC478/TM6C, Sb[1] cu[1]/$NASP^1$

320 **CRISPR mutagenesis**

321 To generate a null allele of *NASP*, a single gRNA targeting exon 2 of the *CG8223* was cloned into

322 pU6-BbsI plasmid as described(Gratz et al. 2015). The gRNA was identified using the DRSC Find

323 CRISPRs tool (http://www.flyrnai.org/crispr2/index.html). The gRNA-expressing plasmid was

324 injected into a *nos-Cas9* expression stock (Best Gene Inc.). Surviving adults were individually

325 crossed to *TM3*/*TM6* balancer stock and progeny were screened by Sanger sequencing. The

326 $NASP^1$ allele contains a 6bp insertion resulting in a two amino acid insertion at amino acid

327 203. $NASP^2$ allele contains a 4bp deletion that results in a frameshift starting at amino acid 203

328 and a premature truncation of NASP. Sequences can be found in S1A Fig.

329 **Antibodies and antibody production**

330 The NASP ORF was cloned into the 6His-MBP-containing expression vector pLM302 (Vanderbilt

331 Center for Structural Biology). 6His-MBP- tagged NASP was expressed in *E. coli* Rossetta DE3 cells

332 (Millipore Sigma, Cat# 71400-3) and purified using MBP Agarose beads (Qiagen). The purified

333 protein was used for injection (Cocalico Biologicals Inc.). NASP antiserum was produced in

334 rabbits. Rabbit anti-NASP antibody was used for western blot (1:2000) and immunoprecipitation.

335 **Protein alignment and structural prediction**

Protein sequence alignments were performed with MAFFT (default settings) and visualized on Jalview. Sequence identities and similarities were generated on SIAS (http://imed.med.ucm.es/Tools/sias.html) with default settings.

The structure of human NASP was previously solved by X-ray crystallography(Bao et al. 2022).The structure of Drosophila NASP was predicted using the AlphaFold Protein Structure Database (Q9I7K6). The α-89 was manually removed from the PDB files using PDBTOOLS(Rodrigues et al. 2018; Honorato et al. 2021; Jiménez-García et al. 2021). Superimposition and RSD values were generated with USCF Chimera. Superimposition was performed on Matchmaker with default settings.

Viability and sterility assays

For viability assays, *NASP*^{1} or *NASP*^{2} virgin females were crossed with male *Df(3R)* flies. The genotype of adult progeny was identified using visible markers. The percentage of viability was calculated as (#observed/# expected) *100. For sterility assays, *NASP*^{1}*/ Df(3R) or NASP*^{2}*/Df(3R)* females or males were incubated with *OrR* males or *OrR* virgin females, respectively. After three days, adult flies were removed and the number of pupae were scored on day ten. As a control, *OrR* females were crossed to *OrR* males.

Embryo Hatching Assay

Embryos laid by *NASP*^{1}*/ Df(3R) or NASP*^{2}*/Df(3R)* mothers were collected on grape juice agar plates with wet yeast. On hundred 0–24-hour after egg laying (AEL) unhatched embryos were transferred to a fresh grape juice plate and incubated at 25°C overnight. Unhatched embryos were scored after 24 hours of incubation. Four hundred embryos were scored for each genotype.

Copy Number Profiling

Ovaries were dissected from *NASP*^{1}*/ Df(3R), NASP*^{2}*/Df(3R)* or *OrR* females fattened for two days on wet yeast in Ephrussi Beadle Ringers (EBR). Stage 13 egg chambers were isolated, re-suspended in LB3 (MacAlpine et al. 2010) and sonicated using a Bioruptor 300 (Diagenode) for five cycles of 30s on and 30s off at maximal power. Lysates were treated with RNase and Proteinase K and genomic DNA was isolated via phenol-chloroform extraction. qPCR was performed using primers previously described (Claycomb et al. 2002).

Cytology and microscopy

NASP^{2}*/Df(3R) or OrR* female flies were incubated with *OrR* male flies in a bottle capped by a grape juice agar plate with wet yeast for embryo collection. Collection plates were changed one hour prior to collections. 0–2 hour (AEL) embryos were collected, dechorionated by 50% bleach for two minutes. Embryos were thoroughly washed with water then dried for 30s. Embryos were transferred to a scintillation vial containing 1mL of heptane. An equal volume of methanol was added and the vial was vigorously shaken by hand for two minutes. Embryos were allowed to settle; the heptane layer was removed and embryos were quickly rinsed with methanol thrice. Embryos were kept in methanol at 4°C until staining. Once ready for staining, embryos were gradually rehydrated in increasing concentration of PBS (18.6mM NaH_2PO_4 ,84.1mM Na_2HPO_4, 1.75M NaCl,pH 7.4). Embryos were then rinsed in PBX (18.6mM NaH_2PO_4 ,84.1mM Na_2HPO_4, 1.75M NaCl, 0.1% Triton X-100, pH 7.4) for five minutes on a nutator. Then, embryos were stained with DAPI (1ug/mL) in PBS for 15 minutes at room temperature. After staining, embryos were washed with PBX for one hour and mounted with VECTASHIELD mounting medium (Vector Laboratories, H-1200). Images were taken at 20X on an Olympus FV-1000 Inverted Confocal Microscope. All 3D images were rendered to one plane via Average intensity projection on Fiji for

visualization. Embryos were manually staged(Kotadia et al. 2010)and scored for morphological defects.

Tissue collection and western blotting

NASP^{1}/ Df(3R) or NASP^{2}/Df(3R) female flies were fatted on wet yeast for 3-4 days, ovaries were dissected in EBR and stage 14 egg chambers were isolated. For embryo isolation, 0-2 hour (AEL) embryos were collected from *NASP^{1}/ Df(3R) or NASP^{2}/Df(3R)* mothers as described above. Embryos and egg chambers were homogenized with a pestle in 2x Lammeli buffer (Bio-Rad, 1610737) supplemented with 50mM DTT, boiled for five minutes and loaded onto a Mini-PROTEAN TGX Stain-Free Gel (Bio-Rad). After electrophoresis, the gel was activated and imaged using a BioRad ChemiDoc™ MP Imaging System following manufacturer recommendations. Protein was transferred to a low fluorescence PVDF membrane using a Trans-Blot Turbo Transfer System (Bio-Rad). Membranes were blocked with 5% milk in TBS-T (140mM NaCl, 2.5mM KCl, 50 mM Tris HCl pH 7.4, 0.1% Tween-20) for 10 minutes. Blots were incubated with the primary antibody (anti-NASP-1:2000, anti-H3-1:000, anti-H2B-1:1000) for one hour at room temperature. Blots were washed three times with TBS-T then incubated with the secondary antibody (HRP anti-mouse-1:20,000, HRP anti-Rabbit-1:25,000) for 30 minutes at room temperature. After hybridization, blots were washed three times with TBS-T then incubated with Clarity ECL solution (Bio-Rad) before imaging. All blots were imaged on the BioRad ChemiDoc™ MP Imaging System.

Immunoprecipitation and Western blotting

Embryos from OrR flies were collected from a population cage. Plates were cleared for one hour, then 0–2 hour embryos (AEL) (pre-MBT) were collected, dechorionated in 50% bleach and flash frozen in nitrogen. Embryo staging was confirmed by DAPI staining (Supplemental 1C). Embryos

were disrupted by grinding them with a mortar and pestle in liquid nitrogen. The powdered embryos were thawed and resuspended on ice in NP40 lysis buffer (50mM Tris-Cl pH 7.4, 150mM NaCl, 1% NP40, 1mM EDTA, 1mM EGTA) supplemented with 2X cOmplete™ Protease Inhibitor Cocktail EDTA-free (Millipore Sigma). Once thawed, the extract was treated with benzonase at a final concentration of 30 U/ml (EMD Millipore, 70664-10KUN) for 30 minutes on ice. After benzonase treatment, extract was centrifuged at 4000xg for five minutes. Supernatant was used as the starting material for immunoprecipitations. Rabbit IgG (negative control) or NASP serum were added to lysates and incubated at 4°C for two hours. After antibody incubation, prewashed Protein A Dynabeads™ (Thermo Fisher Scientific, 10001D) were added to the extract and incubated for one hour at 4°C on a nutator. After incubation, beads were isolated and washed once with NP40 lysis buffer, twice with NP40 lysis high salt wash buffer (50mM Tris-Cl pH 7.4, 500mM NaCl, 1% NP40, 1mM EDTA, 1mM EGTA), and once again with NP40 lysis buffer. Beads were then resuspended in 2x Laemmli sample buffer (Bio-Rad, 1610737) supplemented with 50mM DTT and boiled for five minutes to elute protein. Western blot analysis was performed as described previously (Tissue collection and western blotting).

Mass spectrometry sample preparation

For NASP-immunoprecipitation (IP), samples were prepared as described previously (Immunoprecipitation and Western blotting). For total protein levels in stage 14 egg chambers and embryos, 20 embryos or stage 14 egg chambers were collected for each replicate, flash frozen, and stored at –80°C until use. Once all samples for four biological replicates were collected, samples were thawed on ice and a 100 µL of NP40 lysis buffer was added. Samples were then homogenized ten times with a B-type pestle, transferred into a 1.5mL Eppendorf tube

and centrifuged for 30s at 10,000RCF at 4°C. 100 µL of supernatant was transferred to a new 1.5mL Eppendorf tube for protein precipitation.

Both lysate and IP samples were precipitated using mass spectrometry grade methanol:chloroform:water (3:1:3) and washed three times with methanol. Each wash was followed by a two minute spin at 10,000xg at room temperature. Protein pellets were air dried and resuspended in 5µL of 1% Rapigest SF (Waters). Resuspended proteins were diluted with 32.5 µL mass spectrometry grade water and 10 µL 0.5 M HEPES (pH 8.0), then reduced with 0.5 µL of 0.5 M TCEP (freshly made) for 30 minutes at room temperature. Free sulfhydryl groups were acetylated with 1 µL of fresh 0.5 M Iodoacetamide for 30 minutes at room temperature in the dark and digested with 0.5 µg trypsin/Lys-C (Thermo Fisher) overnight at 37°C shaking. Digested peptides were diluted to 60 µL with water and labeled for 1 hour at room temperature using 16plex TMTpro (Thermo Scientific) or 10plex TMT (Thermo Scientific) for lysate and IP samples, respectively. Labeling was quenched with the addition of fresh ammonium bicarbonate (0.4% v/v final) for one hour at room temperature. Samples were pooled, acidified to pH < 2.0 using formic acid, concentrated to 1/6th original volume via Speed-vac, and diluted back to the original volume with buffer A (95% water, 5% acetonitrile, 0.1% formic acid). Cleaved Rapigest products were removed by centrifugation at 17,000xg for 30 minutes and supernatant transferred to fresh tubes for storage at -80°C until mass spectrometry analysis.

MudPIT liquid chromatography-tandem mass spectrometry

Triphasic MudPIT columns were prepared as previously described using alternating layers of 1.5cm C18 resin, 1.5cm SCX resin, and 1.5cm C18 resin(Fonslow et al. 2012). Pooled TMT samples (roughly one-third of pooled IP samples and roughly 20 µg of peptide from lysate samples) were

loaded onto the microcapillaries using a high-pressure chamber, followed by a 30 minute wash in buffer A (95% water, 5% acetonitrile, 0.1% formic acid). Peptides were fractionated online by liquid chromatography using an Ultimate 3000 nanoLC system and subsequently analyzed using an Exploris480 mass spectrometer (Thermo Fisher). The MudPIT columns were installed on the LC column switching valve and followed by a 20cm fused silica microcapillary column filled with Aqua C18, 3µm, C18 resin (Phenomenex) ending in a laser-pulled tip. Prior to use, columns were washed in the same way as the MudPIT capillaries. MudPIT runs were carried out by 10µL sequential injections of 0, 10, 20, 40, 60, 80, 100 % buffer C (500mM ammonium acetate, 94.9% water, 5% acetonitrile, 0.1% formic acid) for IP samples and 0, 10, 20, 30, 40, 50, 60, 70, 80, 90, 100% buffer C for global lysate samples, followed by a final injection of 90% C, 10% buffer B (99.9% acetonitrile, 0.1% formic acid v/v). Each injection was followed by a 130 min gradient using a flow rate of 500nL/min (0-6 min: 2% buffer B, 8 min: 5% B, 100 min: 35% B, 105min: 65% B, 106-113 min: 85% B, 113-130 min: 2% B). ESI was performed directly from the tip of the microcapillary column using a spray voltage of 2.2 kV, an ion transfer tube temperature of 275°C and a RF Lens of 40%. MS1 spectra were collected using a scan range of 400-1600 m/z, 120k resolution, AGC target of 300%, and automatic injection times. Data-dependent MS2 spectra were obtained using a monoisotopic peak selection mode: peptide, including charge state 2-7, TopSpeed method (3s cycle time), isolation window 0.4 m/z, HCD fragmentation using a normalized collision energy of 36% (TMTpro) or 32% (TMT 10plex), resolution 45k, AGC target of 200%, automatic (lysate) or 150 ms (IP) maximum injection times, and a dynamic exclusion (20 ppm window) set to 60s.

Peptide identification and quantification

Identification and quantification of peptides were performed in Proteome Discoverer 2.4 (Thermo Fisher) using a UniProt *Drosophila melanogaster* proteome database (downloaded February 6th, 2019) containing 21,114 protein entries. The database was adjusted to remove splice-isoforms and redundant proteins and supplemented with common MS contaminants. Searches were conducted with Sequest HT using the following parameters: trypsin cleavage (maximum 2 missed cleavages), minimum peptide length 6 AAs, precursor mass tolerance 20ppm, fragment mass tolerance 0.02 Da, dynamic modifications of Met oxidation (+15.995 Da), protein N-terminal Met loss (-131.040 Da), and protein N-terminal acetylation (+42.011 Da), static modifications of TMTpro (+304.207 Da) or TMT 10plex (+229.163 Da) at Lys and N-termini and Cys carbamidomethylation (+57.021 Da). Peptide IDs were filtered using Percolator with an FDR target of 0.01. Proteins were filtered based on a 0.01 FDR, and protein groups were created according to a strict parsimony principle. TMT reporter ions were quantified considering unique and razor peptides, excluding peptides with co-isolation interference greater that 25%. Peptide abundances were normalized based on total peptide amounts in each channel, assuming similar levels of background in the IPs. Protein quantification used all quantified peptides. Post-search filtering was done to include only proteins with two identified peptides. Unique peptides for each canonical and variant histone was manually identified, summed, and statistically analyzed on Graphpad Prism. For IP samples, multiple t-test was performed ($p<0.05$). For lysate samples, multiple t-test with Holm-Sidak correction was performed ($p<0.05$).

ACKNOWLEDGMENTS

We thank Jacki Hao for assistance in generating the *NASP* mutants. Methodology animations were created by Biorender.com. Confocal imaging and analysis were performed in part with the VUMC Cell Imaging Shared Resource (supported by NIH grants CA68485, DK20593, DK58404, HD15052, DK59637). We thank Amanda Amodeo and Andrea Page-McCaw for critical feedback on this manuscript. This work was supported by National Institutes of Health (NIH) General Medical Sciences awards R35GM133552 to L.P. and R35GM128650 to J.T.N. J.P.D. was supported by R35GM133552.

AUTHOR CONTRIBUTION

R.T. Conceptualization, Formal Analysis, Investigation, Writing – Original Draft, Visualization; **J.P.D**. Investigation, Formal Analysis, Writing – Review & Editing; ; **L.P.** Formal Analysis, Writing – Review & Editing ;**J.T.N.** Conceptualization, Writing – Original Draft, Supervision, Funding acquisition

CONFLICT OF INTEREST

The authors declare no conflict of interest.

REFERENCES

1. Ambrosio L, Schedl P. 1985. Two discrete modes of histone gene expression during oogenesis in *Drosophila melanogaster*. Dev Biol. doi:10.1016/0012-1606(85)90447-6.
2. Arents G, Moudrianakis EN. 1993. Topography of the histone octamer surface: Repeating structural motifs utilized in the docking of nucleosomal DNA. *Proc Natl Acad Sci U S A*. doi:10.1073/pnas.90.22.10489.
3. Au WC, Crisp MJ, DeLuca SZ, Rando OJ, Basrai MA. 2008. Altered dosage and mislocalization of histone H3 and Cse4p lead to chromosome loss in *Saccharomyces cerevisiae*. *Genetics*. doi:10.1534/genetics.108.088518.

4. Bannister AJ, Kouzarides T. 2011. Regulation of chromatin by histone modifications. *Cell Res*. doi:10.1038/cr.2011.22.
5. Bao H, Carraro M, Flury V, Liu Y, Luo M, Chen L, Groth A, Huang H. 2022. NASP maintains histone H3–H4 homeostasis through two distinct H3 binding modes. *Nucleic Acids Res*. 50(9):5349–5368. doi:10.1093/nar/gkac303.
6. Berloco M, Fanti L, Breiling A, Orlando V, Pimpinelli S. 2001. The maternal effect gene, abnormal oocyte (abo), of *Drosophila melanogaster* encodes a specific negative regulator of histones. *Proc Natl Acad Sci U S A*. doi:10.1073/pnas.211428798.
7. Bonner WM, Wu RS, Panusz HT, Muneses C. 1988. Kinetics of Accumulation and Depletion of Soluble Newly Synthesized Histone in the Reciprocal Regulation of Histone and DNA Synthesis. *Biochemistry*. doi:10.1021/bi00417a052.
8. Brown JB, Boley N, Eisman R, May GE, Stoiber MH, Duff MO, Booth BW, Wen J, Park S, Suzuki AM, et al. 2014. Diversity and dynamics of the Drosophila transcriptome. *Nature*. doi:10.1038/nature12962.
9. Camerini-Otero RD, Sollner-Webb B, Felsenfeld G. 1976. The organization of histones and DNA in chromatin: Evidence for an arginine-rich histone kernel. *Cell*. doi:10.1016/0092-8674(76)90145-8.
10. Celona B, Weiner A, Di Felice F, Mancuso FM, Cesarini E, Rossi RL, Gregory L, Baban D, Rossetti G, Grianti P, et al. 2011. Substantial Histone reduction modulates Genomewide nucleosomal occupancy and global transcriptional output. *PLoS Biol.* doi:10.1371/journal.pbio.1001086.
11. Chari S, Wilky H, Govindan J, Amodeo AA. 2019. Histone concentration regulates the cell cycle and transcription in early development. *Dev*. doi:10.1242/dev.177402.
12. Claycomb JM, MacAlpine DM, Evans JG, Bell SP, Orr-Weaver TL. 2002. Visualization of replication initiation and elongation in Drosophila. *J Cell Biol*. 159(2):225–236. doi:10.1083/jcb.200207046.
13. Cook AJL, Gurard-Levin ZA, Vassias I, Almouzni G. 2011. A Specific Function for the Histone Chaperone NASP to Fine-Tune a Reservoir of Soluble H3-H4 in the Histone Supply Chain. Mol *Cell*. doi:10.1016/j.molcel.2011.11.021.
14. Elsässer SJ, Huang H, Lewis PW, Chin JW, Allis CD, Patel DJ. 2012. DAXX envelops a histone H3.3-H4 dimer for H3.3-specific recognition. *Nature*. doi:10.1038/nature11608.
15. Foe VE, Odell GM, Edgar B a. 1993. Timetable of Drosophila Early Development. *Dev*
16. Fonslow BR, Niessen SM, Singh M, Wong CCL, Xu T, Carvalho PC, Choi J, Park SK, Yates JR. 2012. Single-step inline hydroxyapatite enrichment facilitates identification and quantitation of phosphopeptides from mass-limited proteomes with MudPIT. *J Proteome Res*. doi:10.1021/pr300200x.
17. Gratz SJ, Rubinstein CD, Harrison MM, Wildonger J, O'Connor-Giles KM. 2015. CRISPR-Cas9 genome editing in Drosophila. *Curr Protoc Mol Biol*. doi:10.1002/0471142727.mb3102s111.
18. Günesdogan U, Jäckle H, Herzig A. 2010. A genetic system to assess in vivo the functions of histones and histone modifications in higher eukaryotes. *EMBO Rep*. doi:10.1038/embor.2010.124.
19. Gunjan A, Paik J, Verreault A. 2006. The emergence of regulated histone proteolysis. *Curr Opin Genet Dev*. doi:10.1016/j.gde.2006.02.010.
20. Gunjan A, Verreault A. 2003. A Rad53 Kinase-Dependent Surveillance Mechanism that Regulates Histone Protein Levels in *S. cerevisiae. Cell.* doi:10.1016/S0092-8674(03)00896-1.
21. Gurard-Levin ZA, Quivy JP, Almouzni G. 2014. Histone chaperones: Assisting histone traffic and

nucleosome dynamics. *Annu Rev Biochem*. doi:10.1146/annurev-biochem-060713-035536.

22. Hammond CM, Strømme CB, Huang H, Patel DJ, Groth A. 2017. Histone chaperone networks shaping chromatin function. *Nat Rev Mol Cell Biol*. doi:10.1038/nrm.2016.159.
23. Herrero AB, Moreno S. 2011. Lsm1 promotes genomic stability by controlling histone mRNA decay. *EMBO J*. doi:10.1038/emboj.2011.117.
24. Honorato R V., Koukos PI, Jiménez-García B, Tsaregorodtsev A, Verlato M, Giachetti A, Rosato A, Bonvin AMJJ. 2021. Structural Biology in the Clouds: The WeNMR-EOSC Ecosystem. *Front Mol Biosc*i. doi:10.3389/fmolb.2021.729513.
25. Horard B, Loppin B. 2015. Histone storage and deposition in the early Drosophila embryo. *Chromosoma.* doi:10.1007/s00412-014-0504-7.
26. Jiménez-García B, Teixeira JMC, Trellet M, Rodrigues JPGLM, Bonvin AMJJ. 2021. PDB-tools web: A user-friendly interface for the manipulation of PDB files. Proteins *Struct Funct Bioinforma.* doi:10.1002/prot.26018.
27. Khorasanizadeh S. 2004. The Nucleosome: From Genomic Organization to Genomic Regulation. *Cell*. doi:10.1016/S0092-8674(04)00044-3.
28. Kleinschmidt JA, Fortkamp E, Krohne G, Zentgraf H, Franke WW. 1985. Co-existence of two different types of soluble histone complexes in nuclei of *Xenopus laevis* oocytes. *J Biol Chem.* doi:10.1016/s0021-9258(20)71223-8.
29. Kornberg RD. 1974. Chromatin structure: A repeating unit of histones and DNA. *Science* (80-). doi:10.1126/science.184.4139.868.
30. Kornberg RD, Lorch Y. 2020. Primary Role of the Nucleosome. *Mol Cell.* doi:10.1016/j.molcel.2020.07.020.
31. Kotadia S, Crest J, Tram U, Riggs B, Sullivan W. 2010. Blastoderm Formation and Cellularisation in *Drosophila melanogaster* . *In: eLS.* doi: 10.1002/9780470015902.a0001071.pub2
32. Li Z, Johnson MR, Ke Z, Chen L, Welte MA. 2014. Drosophila lipid droplets buffer the H2Av supply to protect early embryonic development. *Curr Biol.* doi:10.1016/j.cub.2014.05.022.
33. Li Z, Thiel K, Thul PJ, Beller M, Kühnlein RP, Welte MA. 2012. Lipid droplets control the maternal histone supply of Drosophila embryos. *Curr Biol*. doi:10.1016/j.cub.2012.09.018.
34. Luger K, Mäder AW, Richmond RK, Sargent DF, Richmond TJ. 1997. Crystal structure of the nucleosome core particle at 2.8 Å resolution. *Nature.* doi:10.1038/38444.
35. MacAlpine HK, Gordân R, Powell SK, Hartemink AJ, MacAlpine DM. 2010. Drosophila ORC localizes to open chromatin and marks sites of cohesin complex loading. *Genome Res.* 20(2):201–211. doi:10.1101/gr.097873.109.
36. Marzluff WF, Wagner EJ, Duronio RJ. 2008. Metabolism and regulation of canonical histone mRNAs: Life without a poly(A) tail. *Nat Rev Genet.* doi:10.1038/nrg2438.
37. Meeks-Wagner D, Hartwell LH. 1986. Normal stoichiometry of histone dimer sets is necessary for high fidelity of mitotic chromosome transmission. *Cell.* doi:10.1016/0092-8674(86)90483-6.
38. Munden A, Wright MT, Han D, Tirgar R, Plate L, Nordman JT. 2022. Identification of replication fork-associated proteins in Drosophila embryos and cultured cells using iPOND coupled to quantitative mass spectrometry. *Sci Rep.* 12(1):1–11. doi:10.1038/s41598-022-10821-9. https://doi.org/10.1038/s41598-022-10821-9.
39. Nabeel-Shah S, Ashraf K, Pearlman RE, Fillingham J. 2014. Molecular evolution of NASP and conserved histone H3/H4 transport pathway. *BMC Evol Biol.* doi:10.1186/1471-2148-14-139.
40. Nagatomo H, Kohri N, Akizawa H, Hoshino Y, Yamauchi N, Kono T, Takahashi M, Kawahara M.

2016. Requirement for nuclear autoantigenic sperm protein mRNA expression in bovine preimplantation development. *Anim Sci J.* doi:10.1111/asj.12538.

41. Natsume R, Eitoku M, Akai Y, Sano N, Horikoshi M, Senda T. 2007. Structure and function of the histone chaperone CIA/ASF1 complexed with histones H3 and H4. *Nature.* doi:10.1038/nature05613.
42. Noll M, Kornberg RD. 1977. Action of micrococcal nuclease on chromatin and the location of histone H1. *J Mol Biol*. doi:10.1016/S0022-2836(77)80019-3.
43. Oliver D, Chalkley R, Granner D. 1974. Identification of a Distinction between Cytoplasmic Histone Synthesis and Subsequent Histone Deposition within the Nucleus. *Biochemistry.* doi:10.1021/bi00701a017.
44. Osley MA. 1991. The regulation of histone synthesis in the cell cycle. *Annu Rev Biochem.* doi:10.1146/annurev.bi.60.070191.004143.
45. Pardal AJ, Fernandes-Duarte F, Bowman AJ. 2019. The histone chaperoning pathway: From ribosome to nucleosome. *Essays Biochem.* doi:10.1042/EBC20180055.
46. Ramos I, Martín-Benito J, Finn R, Bretaña L, Aloria K, Arizmendi JSM, Ausió J, Muga A, Valpuesta JM, Prado A. 2010. Nucleoplasmin binds histone H2A-H2B dimers through its distal face. *J Biol Chem.* doi:10.1074/jbc.M110.150664.
47. Richardson RT, Alekseev OM, Grossman G, Widgren EE, Thresher R, Wagner EJ, Sullivan KD, Marzluff WF, O'Rand MG. 2006. Nuclear autoantigenic sperm protein (NASP), a linker histone chaperone that is required for cell proliferation. *J Biol Chem.* doi:10.1074/jbc.M603816200.
48. Rodrigues JPGLM, Teixeira JMC, Trellet M, Bonvin AMJJ. 2018. pdb-tools: a swiss army knife for molecular structures. *F1000Research.* doi:10.12688/f1000research.17456.1.
49. Shindo Y, Amodeo AA. 2019. Dynamics of Free and Chromatin-Bound Histone H3 during Early Embryogenesis. *Curr Biol.* doi:10.1016/j.cub.2018.12.020.
50. Shindo Y, Amodeo AA. 2021. Report Excess histone H3 is a competitive Chk1 inhibitor that controls cell-cycle remodeling in the early Drosophila embryo. *Curr Biol.* 31(12):2633-2642.e6. doi:10.1016/j.cub.2021.03.035.
51. Singh RK, Kabbaj MHM, Paik J, Gunjan A. 2009. Histone levels are regulated by phosphorylation and ubiquitylation-dependent proteolysis. *Nat Cell Biol*. doi:10.1038/ncb1903.
52. Singh RK, Liang D, Gajjalaiahvari UR, Kabbaj MHM, Paik J, Gunjan A. 2010. Excess histone levels mediate cytotoxicity via multiple mechanisms. *Cell Cycle.* doi:10.4161/cc.9.20.13636.
53. Song Y, Marmion RA, Park JO, Biswas D, Rabinowitz JD, Shvartsman SY. 2017. Dynamic Control of dNTP Synthesis in Early Embryos. *Dev Cell*. doi:10.1016/j.devcel.2017.06.013.
54. Spradling AC, Mahowald AP. 1980. Amplification of genes for chorion proteins during oogenesis in *Drosophila melanogaster*. *Proc Natl Acad Sci U S A*. doi:10.1073/pnas.77.2.1096.
55. Talbert PB, Henikoff S. 2017. Histone variants on the move: Substrates for chromatin dynamics. *Nat Rev Mol Cell Biol.* doi:10.1038/nrm.2016.148.
56. Vastenhouw NL, Cao WX, Lipshitz HD. 2019. The maternal-to-zygotic transition revisited. *Development*. doi:10.1242/dev.161471.
57. Walker J, Bownes M. 1998. The expression of histone genes during *Drosophila melanogaster* oogenesis. *Dev Genes Evol.* doi:10.1007/s004270050144.
58. Wessel SR, Mohni KN, Luzwick JW, Dungrawala H, Cortez D. 2019. Functional Analysis of the Replication Fork Proteome Identifies BET Proteins as PCNA Regulators. *Cell Rep.* doi:10.1016/j.celrep.2019.08.051.

59. Yuan K, Seller CA, Shermoen AW, O'Farrell PH. 2016. Timing the Drosophila Mid-Blastula Transition: A Cell Cycle-Centered View. *Trends Genet.* doi:10.1016/j.tig.2016.05.006.
60. Zhang Z, Krauchunas AR, Huang S, Wolfner MF. 2018. Maternal proteins that are phosphoregulated upon egg activation include crucial factors for oogenesis, egg activation and embryogenesis in *Drosophila melanogaster. G3 Genes, Genomes, Genet.* doi:10.1534/g3.118.200578.
61. Zhao J, Kennedy BK, Lawrence BD, Barbie DA, Gregory Matera A, Fletcher JA, Harlow E. 2000. NPAT links cyclin E-Cdk2 to the regulation of replication-dependent histone gene transcription. *Genes Dev.* doi:10.1101/gad.827700.
62. Zhao R, Zhu Z, Geng R, Jiang X, Li W, Ou G. 2022. Inhibition of histone H3-H4 chaperone pathways rescues *C. elegans* sterility by H2B loss. *PLOS Genet.* 18(6):e1010223. doi:10.1371/journal.pgen.1010223. http://dx.doi.org/10.1371/journal.pgen.1010223.